PHYSICAL REVIEW A **85**, 063409 (2012)

# Strong-field photodetachment of $H^-$ by few-cycle laser pulses

S. F. C. Shearer[1,*] and C. R. J. Addis[2,†]
[1] *Centre for Theoretical Atomic, Molecular and Optical Physics, Queen's University Belfast, Belfast BT7 1NN, Northern Ireland*
[2] *School of Engineering and Physical Sciences, Heriot-Watt University, Edinburgh EH14 4AS, Scotland*

(Received 26 March 2012; revised manuscript received 14 May 2012; published 12 June 2012)

The recent adiabatic saddle-point method of Shearer *et al.* [Phys. Rev. A **84**, 033409 (2011)] is applied to study strong-field photodetachment of $H^-$ by few-cycle linearly polarized laser pulses of frequencies near the two-photon detachment threshold. The behavior of the saddle points in the complex-time plane for a range of laser parameters is explored. A detailed analysis of the influence of laser intensities [$(2 \times 10^{11})$–$(6.5 \times 10^{11})$ $\mathrm{W/cm^2}$], midinfrared laser wavelengths (1800–2700 nm), and various values of the carrier envelope phase (CEP) on (i) three-dimensional probability detachment distributions, (ii) photoangular distributions (PADs), (iii) energy spectra, and (iv) momentum distributions are presented. Examination of the probability distributions and PADs reveal main lobes and jetlike structures. Bifurcation phenomena in the probability distributions and PADs are also observed as the wavelength and intensity increase. Our simulations show that the (i) probability distributions, (ii) PADs, and (iii) energy spectra are extremely sensitive to the CEP and thus measuring such distributions provides a useful tool for determining this phase. The symmetrical properties of the electron momentum distributions are also found to be strongly correlated with the CEP and this provides an additional robust method for measuring the CEP of a laser pulse. Our calculations further show that for a three-cycle pulse inclusion of all eight saddle points is required in the evaluation of the transition amplitude to yield an accurate description of the photodetachment process. This is in contrast to recent results for a five-cycle pulse.

DOI: 10.1103/PhysRevA.85.063409 PACS number(s): 32.80.Rm, 32.80.Gc, 32.80.Qk

## I. INTRODUCTION

Since the turn of the millennium, remarkable advances achieved in laser technology in both the infrared [1] and xuv region [2] have stimulated many experimental and theoretical studies of physical processes that are sensitive to the carrier envelope phase (CEP) of laser pulses (see review articles [3–5] and references therein). In particular, as a result of the availability of few-cycle laser pulses, multiphoton detachment of negative ions in few-cycle pulses has become a subject of contemporary interest in strong-field atomic physics. Until recently the bulk of experimental and theoretical studies of multiphoton detachment of negative atomic ions in strong-field physics have concentrated on long (i.e., many-cycle, periodic) linearly polarized pulses [6–12]. In contrast to long laser pulses, which are characterized completely by their frequency, amplitude, and polarization, ultrashort pulses are characterized by two additional laser parameters, namely, the CEP and the number of optical cycles. These additional laser parameters have provided unique new research tools to probe laser-ion interactions in unprecedented detail from a novel perspective.

To date semianalytical approaches such as the adiabatic saddle-point model of Gribakin and Kuchiev [6] based on the original Keldysh approximation [13] have proven to be very successful in describing quantitatively the interaction of negative atomic ions with strong monochromatic laser fields [7,8,11]. The original Gribakin-Kuchiev (GK) theory, developed for laser fields comprising an infinite number of cycles, consists of neglecting the influence of the core potential on the detached electron and representing the final state by the Volkov wave function [14]. The photodetachment amplitude is obtained using the saddle-point method and given analytically by the contributions of two complex moments of time per period. One of the main strengths of the GK theory is that it yields very reliable quantitative results over a wide range of laser intensities and frequencies for both the perturbative and nonperturbative regimes. Increasing interest in the role the CEP plays in the photodetachment of negative atomic ions in few-cycle laser pulses [15–20] motivated us recently to adapt the GK formalism to ultrashort linearly polarized pulses [21]. There we showed that application of the saddle-point method to the amplitude for a laser pulse with $N$ optical cycles [e.g., of the form $\mathbf{A}(t) \propto \sin^2(\omega t/2N)\sin(\omega t + \alpha)$] produces $2(N+1)$ saddle points in complex time. Our formalism [21] was initially applied to consider multiphoton detachment of $H^-$ in a five-cycle laser pulse with a wavelength of 10.6 $\mu$m and intensities of $10^{10}$, $5 \times 10^{10}$, and $10^{11}$ $\mathrm{W/cm^2}$ with varying CEP. We numerically calculated the spectrum of the photoelectrons as a function of both energy and emission angle as well as the angle integrated energy and total detachment probabilities and examined the influence of the CEP on these distributions.

Increasingly more research effort has concentrated on the experimental and theoretical study of photodetachment dynamics of negative ions by few-cycle pulses in the midinfrared region between 800 and 2700 nm, corresponding to photon energies between 1.55 and 0.49 eV and laser frequencies of 0.0570–0.0169 a.u. [12,17–20,22,23]. Under the influence of this range of laser parameters the process of electron photodetachment near the two-photon threshold [12,18] for $H^-$ becomes dominant. In light of the current interest for this range of laser parameters we apply our recent model [21] to consider an in depth study of strong-field near-threshold photodetachment of $H^-$ for a range of laser intensities between

---

[*] f.shearer@qub.ac.uk

[†] ca99@hw.ac.uk

©2012 American Physical Society

$2\times 10^{11}$ and $6.5\times 10^{11}$ W/cm$^2$ and laser wavelengths between 1800 and 2700 nm as well as varying the CEP for a three-cycle laser pulse. These calculations provide valuable insight into the physical picture of [few-femtosecond laser pulses in the midinfrared region (i.e., pulse duration between 21 and 27 fs)] ionization dynamics. In this paper we investigate the behavior of the saddle points that correspond to the different (complex-valued) moments of time that electron detachment occurs and their contribution to the transition amplitude. We find that the density distribution of saddle points in the complex plane is sensitive to laser intensity, frequency, and CEP but independent of pulse length. From the transition amplitude we then investigate the dependence of various laser parameters on the (i) three-dimensional (3D) probability detachment distributions, (ii) photoangular distributions (PADs), (iii) electron energy spectra, and (iv) photoelectron momentum distributions. We find that the presence of the two-photon threshold plays a significant role in determining the behavior of these distributions. The calculations are compared with available theoretical results [12,18,21,22] and experimental data [7].

This paper is organized as follows. In Sec. II we give a brief overview of our theoretical model. This is based on the adiabatic saddle-point approach of Gribakin and Kuchiev [6], which we have extended recently in Ref. [21] to describe multiphoton detachment of the negative H$^-$ ion in a few-cycle laser pulse. In Sec. III we present the results of our numerical calculations and their analysis. Our work shows that the adiabatic saddle-point method in Ref. [21] achieves an accuracy that is comparable to the most sophisticated numerical methods and works exceptionally well outside its formal applicability range. Finally, in Sec. IV we summarize our results and discuss our conclusions. Atomic units are used throughout unless stated otherwise.

## II. THEORY

The presence of only a single bound state in H$^-$ allows for an accurate theoretical treatment of photodetachment by few-cycle laser pulses within the adiabatic saddle-point method of Shearer *et al.* [21]. We consider the detachment of the valence electron from H$^-$ by the ir laser field

$$\mathbf{F}(t) = -\frac{d\mathbf{A}}{dt}, \tag{1}$$

where we assume that the laser is polarized along the $\hat{\mathbf{z}}$ axis whose time-dependent vector potential is given by

$$\mathbf{A}(t) = A(t)\hat{\mathbf{z}} = A_0\left[\sin^2\left(\frac{\omega t}{2N}\right)\sin(\omega t+\alpha)\right]\hat{\mathbf{z}}. \tag{2}$$

Here $\omega$ is the frequency of the pulse, $N$ is the number of optical cycles in the pulse, and $\alpha$ is the CEP. The peak value $A_0$ of the vector potential $\mathbf{A}(t)$ is related to the peak laser intensity $I_0$ by

$$A_0 = \sqrt{I_0/I_{\text{a.u.}}}/\omega = F_0/\omega, \tag{3}$$

where $I_{\text{a.u.}} = 3.515\times 10^{16}$ W/cm$^2$ and $F_0$ is the peak value of the electric field strength. It is useful to note that the component of the vector potential $\mathbf{A}(t)$ of the $\sin^2$ $N$-cycle laser pulse in the $\hat{\mathbf{z}}$ direction is composed of three quantized frequency components and thus may be written in the form

$$A(t) = \frac{A_0}{4}[2\sin(\omega_1 t+\alpha) - \sin(\omega_2 t+\alpha) - \sin(\omega_3 t+\alpha)], \tag{4}$$

where $\omega_1=\omega$, $\omega_2=\omega(1+\frac{1}{N})$, and $\omega_3=\omega(1-\frac{1}{N})$. The photoelectron spectrum for the $N$-cycle laser pulse in the laser field $\mathbf{F}(t)$ is determined by the differential detachment probability

$$dw = 2|A_{\mathbf{p}}|^2\frac{d^3p}{(2\pi)^3}, \tag{5}$$

where the factor of 2 accounts for the two electrons in the hydrogen negative ion. From Ref. [21] the photodetachment amplitude $A_{\mathbf{p}}$ of electron ejection with momentum $\mathbf{p}$ and pulse duration $\tau = 2\pi N/\omega$ is given by

$$A_{\mathbf{p}} = \int_0^{\tau}\left[E_0 - \frac{1}{2}(\mathbf{p}+\mathbf{k}_t)^2\right]\tilde{\Phi}(\mathbf{p}+\mathbf{k}_t) \times \exp\left[\frac{i}{2}\int^{t}(\mathbf{p}+\mathbf{k}_{t'})^2dt' - iE_0t\right]dt, \tag{6}$$

where $\mathbf{k}_t$ is the classical electron momentum due to the field given by

$$\mathbf{k}_t = -\int^{t}\mathbf{F}(t')dt' \tag{7}$$

and

$$\tilde{\Phi}(\mathbf{q}) = \int e^{-i\mathbf{q}\cdot\mathbf{r}}\Phi_0(\mathbf{r})d\mathbf{r} \tag{8}$$

is the Fourier transform of $\Phi_0(\mathbf{r})$. For H$^-$ (see Ref. [21]) we have that

$$\tilde{\Phi}(\mathbf{p}+\mathbf{k}_t) \simeq \frac{\sqrt{4\pi}B}{(\mathbf{p}+\mathbf{k}_t)^2+\kappa^2}, \tag{9}$$

where $B$ is a normalization constant. The integrand in Eq. (6) contains a rapidly oscillating exponent $\exp[if(t)]$, where

$$f(t) = \frac{1}{2}\int^{t}(\mathbf{p}+\mathbf{k}_{t'})^2dt' - E_0t \tag{10}$$

and hence the integral over time in Eq. (6) can be evaluated using the saddle-point method (see, e.g., Ref. [21]). Thus we obtain

$$A_{\mathbf{p}} = -\sum_{\mu}\frac{\pi\sqrt{2}B}{\sqrt{-if''(t_\mu)}}\exp[if(t_\mu)], \tag{11}$$

where the sum is over all saddle points $t_\mu$. The saddle points $t_\mu$ are the complex roots of $f'(t)=0$ given by solution of

$$(\mathbf{p}+\mathbf{k}_t)^2+\kappa^2 = 0, \tag{12}$$

where $\kappa$ parametrizes the binding energy $|E_0|\equiv\kappa^2/2$. In accordance with the theory of adiabatic transitions, only the saddle points in the upper half plane of complex $t$ are taken into account in Eq. (11). The saddle points correspond physically to the coherent emission of the photoelectron at different complex moments of time. Explicit expressions for $f(t_\mu)$ and $f''(t_\mu)$ in Eq. (11) for the $\sin^2$ $N$-cycle laser pulse are given in Ref. [21].

For a short laser pulse with $N$ optical cycles and a sin$^2$ envelope as considered here, Eq. (12) takes the form

$$\left[\mathbf{p}+\frac{\mathbf{F}}{\omega}\sin^2\left(\frac{\omega t}{2N}\right)\sin(\omega t+\alpha)\right]^2+\kappa^2=0. \tag{13}$$

Reducing the saddle-point equation (13) to scalar form and setting $\phi=\omega t$ yields

$$p^2+\frac{2pF\cos\theta}{\omega}\sin^2\left(\frac{\phi}{2N}\right)\sin(\phi+\alpha)+\frac{F^2}{\omega^2}\sin^4\left(\frac{\phi}{2N}\right)\sin^2(\phi+\alpha)+\kappa^2=0, \tag{14}$$

where $\theta$ is the angle between the photoelectron momentum **p** and the field **F**. As has been shown in Ref. [21], numerical solution of this equation for H$^-$ yields $2(N+1)$ complex roots, where $2N$ of the roots arise from the laser frequency $\omega_1$ and the additional two roots arise from the frequencies $\omega_2$ and $\omega_3$, respectively. Finally in this section we give formulas to calculate the photoelectron energy spectrum

$$\frac{dw}{d\varepsilon}=2\pi\int_0^\pi\frac{dw}{d\varepsilon d\Omega}\sin\theta d\theta \tag{15}$$

and total detachment probability

$$w=\int_0^\infty\frac{dw}{d\varepsilon}d\varepsilon. \tag{16}$$

## III. NUMERICAL RESULTS AND DISCUSSION

In this section we use the formulas derived in Sec. II to consider photodetachment of H$^-$. To apply our theory to H$^-$ we need the numerical values of the asymptotic parameters $B$ and $\kappa$ of the corresponding bound-state wave functions. In our calculations the value of $B$ is taken from Ref. [24] and the value of $\kappa$ is calculated from the corresponding binding energy as $\kappa=\sqrt{2|E_0|}$ using Ref. [25]. In these calculations we assume a laser pulse with $N=3$ optical cycles. We consider pulses with three peak intensities $I_0=2\times10^{11}$, $4\times10^{11}$, and $6.5\times10^{11}$ W/cm$^2$ for each of the three laser wavelengths $\lambda=2150$, 2400, and 2700 nm with CEP values of $\alpha=0$, $\pi/4$, and $3\pi/2$, respectively. The corresponding saddle points of Eq. (14) in each case are initially obtained by considering the 3D surface plots of $|f'(\phi)|^{-1/2}$, so the roots of Eq. (14) are visualized as infinities rather than zeros. The surface plots for each of the three peak intensities $I_0$ are considered at $\lambda=2150$, 2400, and 2700 nm and each $\alpha$ reveals eight saddle points [i.e., eight approximate graphical solutions of the saddle-point equation (14) $N=3$ cycle pulse]. This result is in agreement with Ref. [21]. We then refine the approximate roots found from our graphical solution by using the Newton-Raphson method for complex roots. The numerical calculation involves refining each root in turn for a range of angles $\theta$ between the direction of the laser field and the momentum **p** of the detached electron. In the present calculations we consider $0\leqslant\theta\leqslant180^\circ$ taking a step size of $1^\circ$. The range of photoelectron momenta $\varepsilon$ considered is between $0.05\omega$ and $10\omega$. Our calculations model detachment for laser pulses $\lambda=2150$, 2400, and 2700 nm. These correspond to the laser frequencies $\omega=0.021\,19$, $0.018\,99$, and $0.016\,88$ a.u., respectively. The momentum values $p$ for each frequency ranging from the threshold values (0.046 03, 0.043 57, and 0.041 08 a.u.) to maximum values (0.6510, 0.6162, and 0.5810 a.u.) respectively are obtained by considering $p=\sqrt{2\varepsilon}$ for equally spaced energies $\varepsilon_j=(\omega/20)j$ with $j=1,2,\ldots,201$. In the case of the momentum distributions we consider the additional wavelength of 1800 nm corresponding to the laser frequency 0.025 32 a.u. Finally, the 2D momentum $(p_x,p_y)$ distributions are calculated using Eq. (14), where we take $p_x=p\cos\theta$ and $p_y=p\sin\theta$. We calculate the momentum $(p_x,p_y)$ distributions for low-energy photoelectron momentum $p$ ranging from $-0.3$ to 0.3 a.u., i.e., $E_e\leqslant0.045$ a.u.

### A. Saddle-point "smiles"

Figure 1 shows the eight saddle points that are a solution of Eq. (14) for the three-cycle pulse at a fixed laser intensity of $4\times10^{11}$ W/cm$^2$ for three laser wavelengths 2150, 2400, and 2700 nm and CEP values of $\alpha=0,\pi/4$, and $3\pi/2$, respectively. Further consideration of the behavior of the saddle points to assess the influence of varying the laser intensity is reported in Figs. S1 ($2\times10^{11}$ W/cm$^2$) and S2 ($6.5\times10^{11}$ W/cm$^2$) of Ref. [26] (with the same laser wavelengths and values of the CEP as in Fig. 1).

In Fig. 1 each group of points in each of the nine panels depicts the saddle points for the five energies in the range $0.05\omega\leqslant\epsilon\leqslant10\omega$ and the five angles $\theta=0$, $45^\circ$, $90^\circ$, $135^\circ$, and $180^\circ$ (represented by different colors). As in Ref. [21] the saddle points are distributed in the shape of a smile. A similar pattern is observed in Figs. S1 and S2 of Ref. [26].

In Fig. 1 (and Figs. S1 and S2 of Ref. [26]) it is noted that as the photoelectron energy increases from $0.05\omega$ to $10\omega$ the roots move further into the complex plane and each group of saddle points moves physically closer to the next adjacent group of saddle points, with the first root being the first group of stars on the left-hand side and the eighth root being the last group on the right-hand side. The density of the distribution of saddle points in Fig. 1 (as in Figs. S1 and S2 of Ref. [26]) differs from Ref. [21], where a five-cycle pulse was considered for a laser wavelength of 10.6 $\mu$m for three laser intensities of $10^{10}$, $5\times10^{10}$, and $10^{11}$ W/cm$^2$. Figure 1 in Ref. [21] showed that the 12 saddle points calculated over the same range of photon energies and angles as above occur in quite distinct clusters compared with the present distribution of saddle points in Fig. 1 (and Figs. S1 and S2 of Ref. [26]) for the laser parameters considered in the three-cycle pulse. Further calculations carried out for comparison with the longer wavelength of 10.6 $\mu$m for intensities of $10^{10}$, $5\times10^{10}$, and $10^{11}$ W/cm$^2$ for a three-cycle laser pulse (not presented here) yield a distribution of roots similar to that produced for the five-cycle pulse. This confirms that the separation between groups of adjacent roots calculated over the energy and angular range considered here is independent of the pulse length. The pulse length affects only the range along the real axis in which the smile lies.

Figure 1 also shows that as the wavelength is increased keeping the intensity and CEP fixed, the roots move closer to the real axis. In Fig. 1 we observe for a fixed wavelength and fixed CEP that as the intensity is increased the saddle points move closer to the real axis. Another feature that is the same

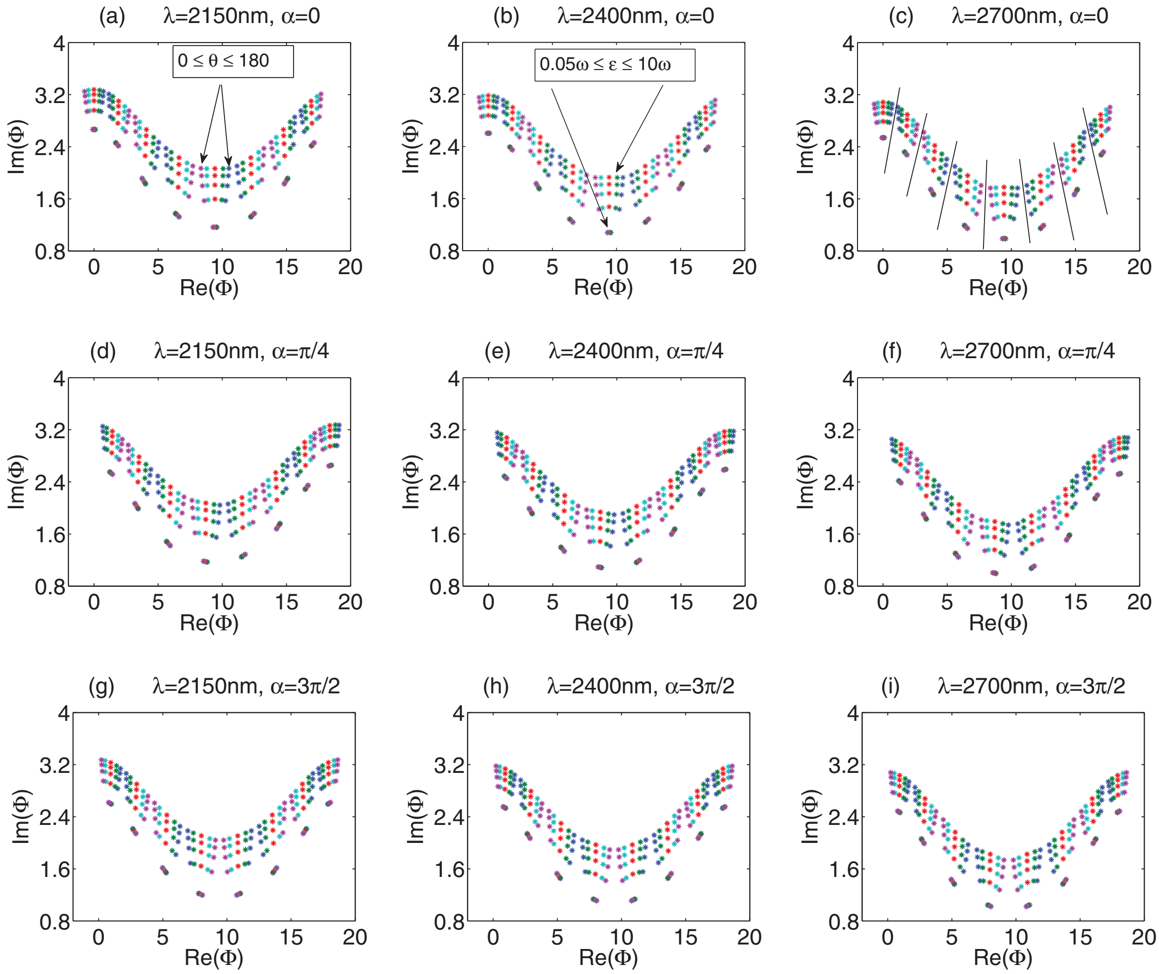

FIG. 1. (Color online) Complex-time saddle points for the three-cycle pulse at a laser intensity of $4 \times 10^{11}$ W/cm$^2$. The panels in each row represent wavelengths of 2150, 2400, and 2700 nm. The panels in each column correspond to a CEP of $\alpha = 0, \pi/4$, and $3\pi/2$. Each group of points represents the position of a saddle point for a range of photoelectron energies from $\varepsilon = 0.05\omega$ to $10\omega$ and angles $\theta = 0, 45^\circ, 90^\circ, 135^\circ$, and $180^\circ$. In each group the points closest to the real axis correspond to the smallest photoelectron energy. Panel (a) highlights the range of angles, panel (b) highlights the range of photon energies, and panel (c) highlights the corresponding group of individual saddle points for the range of $\theta$ and $\varepsilon$ separated by straight lines.

as in Ref. [21] is that the saddle points are closer to the real axis near the middle of the pulse, where the field is strongest. Varying the carrier envelope phase for a fixed wavelength and intensity makes the saddle points slide along the smile, as is depicted in Fig. 1. In particular we note in Fig. 1 that for $\alpha = 0$ the fifth root lies closest to the real axis, for $\alpha = \pi/4$ the fourth root is closest to the real axis, and for $\alpha = 3\pi/2$ the fourth and fifth roots are equally distant from the real axis; that is, the smile distributions are asymmetric for $\alpha = 0$ and $\pi/4$ and symmetric for $3\pi/2$. These results (which are also consistent with the simulations in Figs. S1 and S2 of Ref. [26]) show that the influence of individual saddle points on the transition amplitude will vary as the CEP is altered.

Figure 1 herein and Figs. S1 and S2 of Ref. [26] further show that as the intensity and wavelength are increased the individual groups of saddle points calculated for each of the five photoelectron energies between $0.05\omega$ and $10\omega$ over the angles $\theta = 0{,}45^\circ{,}90^\circ{,}135^\circ$, and $180^\circ$ bunch more closely together and become increasingly separate from the next adjacent group of saddle points. Thus the distribution and shape of the smile is dependent on laser intensity, wavelength, and the CEP. One notable feature in Fig. 1 (and similarly noted in Figs. S1 and S2 of Ref. [26]) is the sizable gap between the roots at the lowest photoelectron energy of $0.05\omega$ compared with the higher electron energies at $2.5375\omega, 5.025\omega, 7.5125\omega$, and $10\omega$. This gap increases for the present intensity as $\lambda$ decreases. Increasing the photoelectron energy moves the saddle points further into the complex plane, thus ejection of photoelectrons with higher energy is less likely. Figure 1 further shows for $\alpha = 0$ that the electron is more likely to be detached parallel to the field rather than perpendicular to it. These observations are in agreement with the results in Ref. [21] for a short laser pulse and Ref. [6] in the case of a long laser pulse.

### B. Photoelectron differential detachment probability

Figure 2 shows the differential detachment probabilities for a three-cycle laser pulse at laser intensities of $2 \times 10^{11}$, $4 \times 10^{11}$, and $6.5 \times 10^{11}$ W/cm$^2$, respectively. The differential

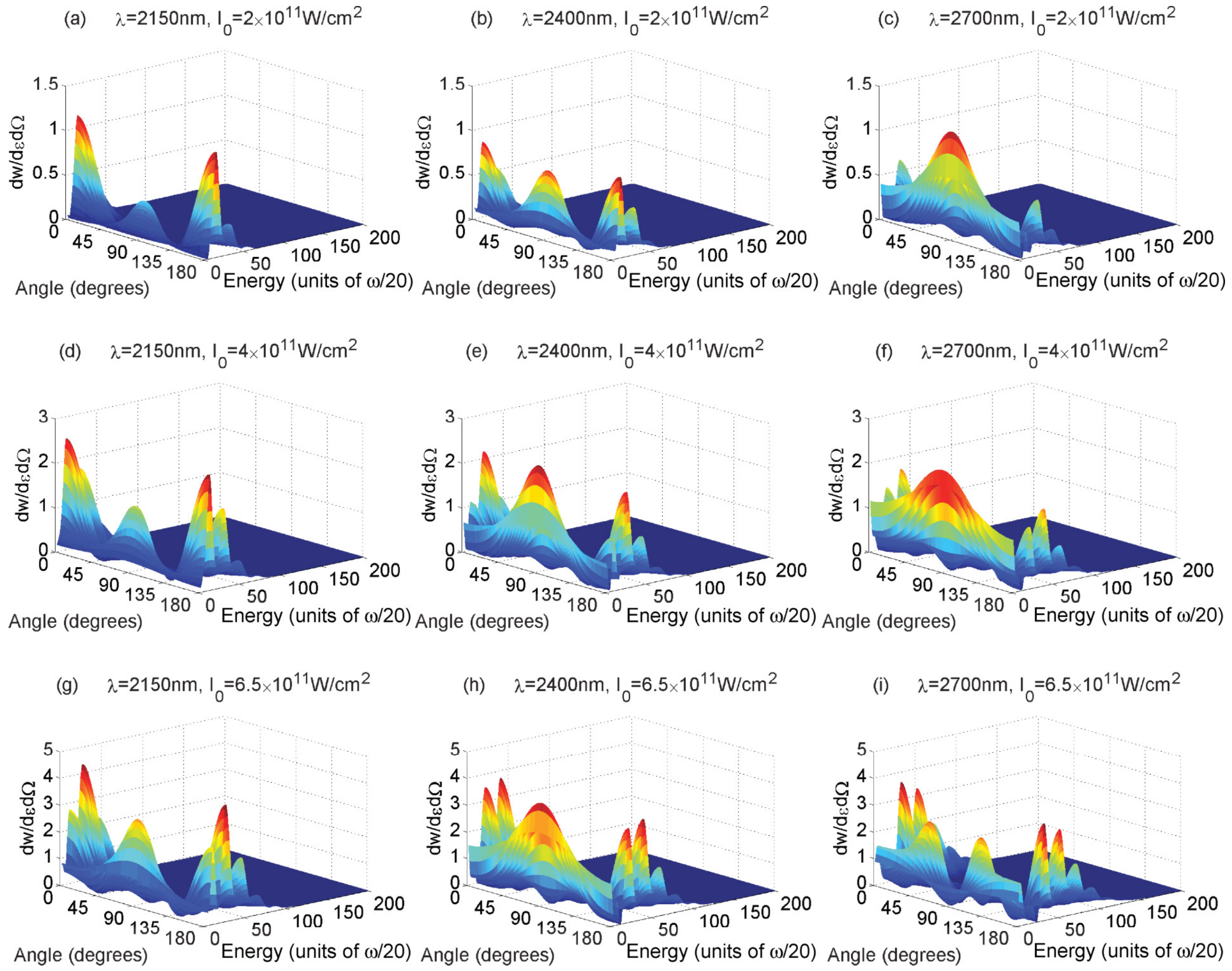

FIG. 2. (Color online) Differential detachment probabilities $dw/d\Omega d\varepsilon$ for the three-cycle pulse calculated with the CEP of $\alpha = 0$. The panels in each row represent wavelengths of 2150, 2400, and 2700 nm. The panels in each column correspond to peak laser intensities of $2 \times 10^{11}$, $4 \times 10^{11}$, and $6.5 \times 10^{11}$ W/cm$^2$. The energy axis in each plot shows the photoelectron energy in units of $\omega/20$.

detachment probabilities at each intensity are investigated by varying the three laser wavelengths of 2150, 2400, and 2700 nm for a fixed CEP of $\alpha = 0$. Similar calculations that highlight the effect of varying the CEP on the differential detachment probability for the same laser intensities and wavelengths as considered in Fig. 2 are reported in Figs. S3 (for $\alpha = \pi/4$) and S4 (for $\alpha = 3\pi/2$) of Ref. [26].

### *1. Laser-wavelength dependence of the probability distributions*

In Fig. 2(a) for a wavelength of $\lambda = 2150$ nm and intensity of $2 \times 10^{11}$ W/cm$^2$ we see that the height of the two lobes is higher than the central jet. As the wavelength at $2 \times 10^{11}$ W/cm$^2$ is increased the central jet becomes bigger, as seen in Fig. 2(b), and at the highest wavelength of 2700 nm we see that the two lobes have receded and the central jet has become the dominant feature in Fig. 2(c). This pattern is repeated at laser intensities of $4 \times 10^{11}$ W/cm$^2$ [Figs. 2(d)–2(f)]. Figures 2(a)–2(f) further show that the ratio of the height of the central jet to that of the main lobe decreases sharply with increasing wavelength. At a highest intensity of $6.5 \times 10^{11}$ W/cm$^2$ [Figs. 2(g)–2(i)] a more dramatic progression is evident with increasing wavelength. First, at the lowest wavelength of 2150 nm in Fig. 2(g) the ratio of the height of the central jet to that of the side lobes is much smaller in comparison to Figs. 2(a) and 2(d). Second, in Fig. 2(h) the central jet has become the dominant feature at the lower wavelength of 2400 nm, being larger and much broader, in contrast to the findings at the lower intensities of $2 \times 10^{11}$ and $4 \times 10^{11}$ W/cm$^2$ in Figs. 2(b) and 2(e), respectively. Finally, at the highest wavelength of 2700 nm in Fig. 2(i) the disappearance of the central jet has been replaced by the emergence of a central two-jetlike structure accompanied by lobes on either side of this new structure. The behavior reported in Fig. 2 is also reflected at the CEP values of $\alpha = \pi/4$ and $3\pi/2$ in Figs. S3 and S4 of Ref. [26].

### *2. Laser-intensity dependence of the probability distributions*

A notable trend observed in Fig. 2 is that as the laser intensity is increased from $2 \times 10^{11}$ to $4 \times 10^{11}$ W/cm$^2$ [for all wavelengths considered, Figs. 2(a)–2(f)] and $6.5 \times 10^{11}$ [for wavelengths of 2150 and 2400 nm, Figs. 2(g) and 2(h)] the central jets increase and become broader while the dominance of the two side lobes recede. These dominant central jets are a signature of the threshold effect (predicted experimentally by Ref. [7] and confirmed theoretically by Floquet calculations [22] and by the generalized phased Bessel function treatment [12]) where the detached electrons are mainly ejected perpendicular to the laser polarization. At the highest intensity of $6.5 \times 10^{11}$ W/cm$^2$ with $\lambda = 2700$ nm [Fig. 2(i)] it can be seen that a bifurcation phenomenon occurs where the single broad central jet with its maximum at $\pi/2$ for a CEP of $\alpha = 0$ has disappeared and two narrower jets have evolved in its place. The physical behavior underlying this bifurcation in the probability distributions coincides with the two-photon detachment channel closure. Figure 2(i) corresponds to the process of three-photon detachment. It is observed from Fig. 2 that increasing intensity at a fixed wavelength influences the underlying bifurcation phenomenon, but to a lesser degree than increasing the wavelength at a fixed intensity in the present calculations. This behavior reported in Fig. 2 is also reflected at the CEP values of $\alpha = \pi/4$ and $3\pi/2$ in Figs. S3 and S4 of Ref. [26]. A comparison of Fig. 2 and Figs. S3 and S4 in Ref. [26] show that the probability distributions are symmetric for $\alpha = 0$ but are asymmetric for $\alpha = \pi/4$ and $3\pi/2$. It is noted that the behavior of the distributions becomes increasingly asymmetric as the laser intensity increases for the CEP values considered here. Finally, from a comparison of Fig. 2 and Figs. S3 and S4 of Ref. [26] we see that as the fixed laser intensity is increased the probabilities increase for all the wavelengths and values of the CEP considered.

### C. Angular distributions

In this section we discuss the laser wavelength and intensity dependence of PADs of two- and three-photon detachment of H$^-$. We also study the effect of the CEP dependence of PADs for varying laser wavelengths and intensities.

#### 1. *Two and three photon detachment PADs*

To gain more insight into the structure of PADs at above-threshold detachment we investigate their dependence on laser wavelength and laser intensity. In Figs. 3(a)–3(c) at a fixed intensity of $2 \times 10^{11}$ W/cm$^2$ we note that as the wavelength is increased the height of the central jet increases, its peak begins

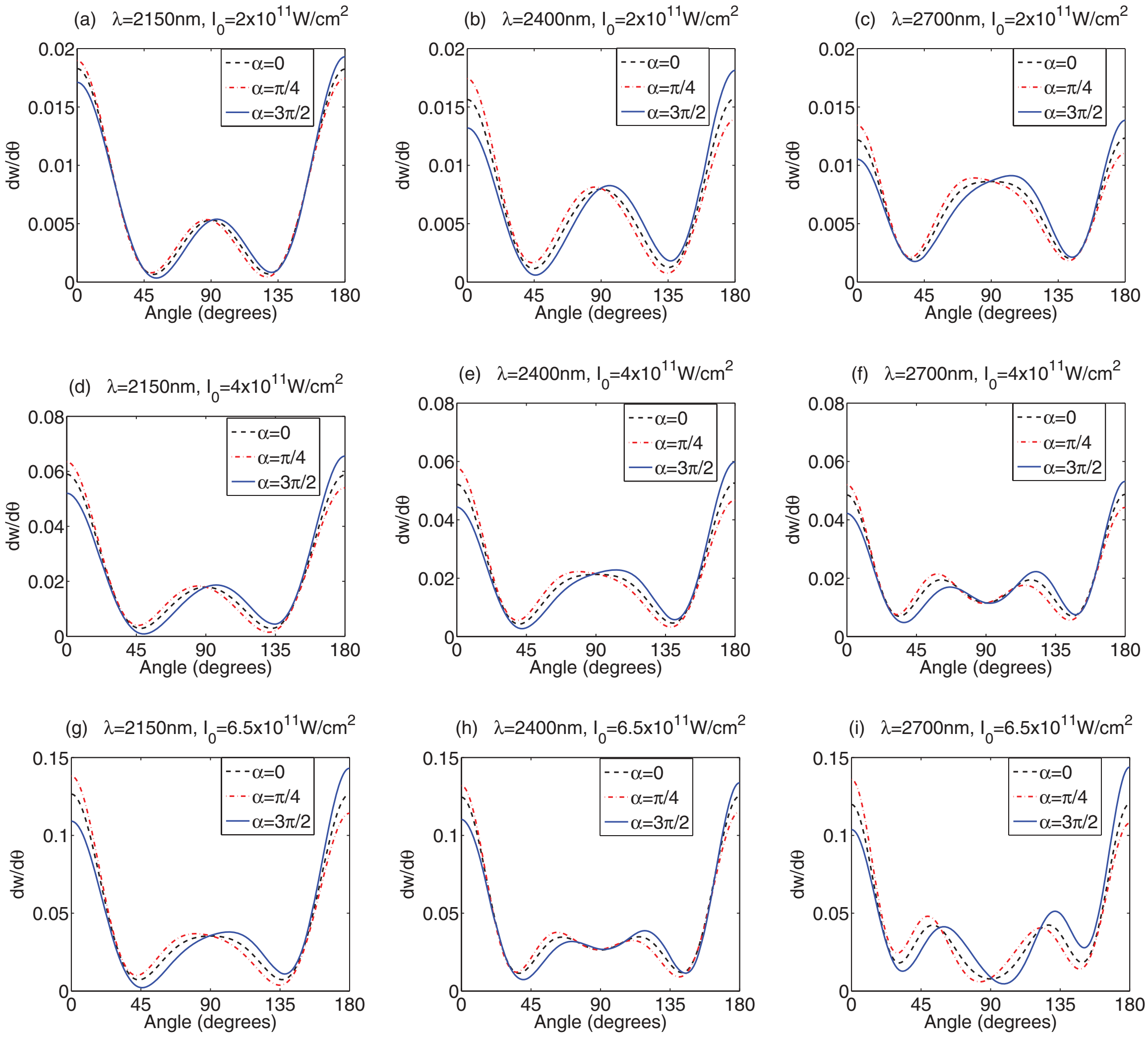

FIG. 3. (Color online) Dependence of the photoelectron angular distribution on the CEP $\alpha$. The panels in each row correspond to the peak laser intensities $2 \times 10^{11}$, $4 \times 10^{11}$, and $6.5 \times 10^{11}$ W/cm$^2$. The panels in each column represent wavelengths of 2150, 2400, and 2700 nm. Panels (a)–(e) and (g) correspond to two-photon detachment while panels (f), (h), and (i) correspond to three-photon detachment.

to flatten out, and the side lobes become less prominent. At the laser intensity of $4 \times 10^{11}$ W/cm$^2$ with increasing wavelength the central jet becomes wider and for a critical bifurcation wavelength between $2400 < \lambda < 2700$ nm its peak eventually becomes flat, which coincides with an isotropic distribution of the detached electrons corresponding to the closure of the two-photon channel. As $\lambda$ is increased beyond the critical bifurcation wavelength the flat peak transforms into a two-peak structure connected by a minimum. This structure corresponds physically to the absorption of three photons. At an intensity of $6.5 \times 10^{11}$ W/cm$^2$ a similar pattern is observed but the single jet begins to split into two jets at a lower critical wavelength in the range $2150 < \lambda < 2400$ nm, where closure of the two-photon detachment channel at this intensity is realized. Figure 3(i) shows the two-peak structure, which has become more firmly established at $\lambda = 2700$ nm, corresponding to the three-photon detachment channel. Our calculations show that the bifurcation phenomenon observed in the PADs is directly influenced by the ponderomotive shift $U_p = I_0/4\omega^2$ increasing. This behavior can be observed directly from the nine panels in Fig. 3 where a higher laser intensity and higher wavelength yield a higher ponderomotive shift and brings the two-photon detachment channel closer to the threshold of channel closure. The critical bifurcation wavelength and intensity of the two-photon detachment is determined from the energy conservation law $E_k = 2\omega - U_p - E_b$ and occurs close to $E_k \rightarrow 0$, where $E_k$ is the final kinetic energy of the detached electron and $E_b$ is the bound-state energy of the H$^-$ ion. This threshold behavior has been previously observed by Reichle *et al.* [7]. Our calculations are also in good qualitative agreement with nonperturbative Floquet calculations [22]. The present calculations, however, extend the range of intensities, wavelengths, and duration of the laser pulse considered by these authors. Also, as in Ref. [12], the two-photon PADs in Figs. 3(a), 3(d), and 3(g), where our chosen range of parameters are close to those of Ref. [12], exhibit a structure consisting of a central jet and two main lobes, one of each located on either side of the central jet. Figures 3(a), 3(d), and 3(g) further show that the ratio of the height of the central jet to that of the main lobe varies in the manner predicted by Bai *et al.* [12]. Figures 3(a)–3(e) and 3(g) illustrate that for $\alpha = 0$ the photoelectrons from the two-photon detachment channel are ejected mostly perpendicular to the laser polarization. This behavior has been observed by Reichle *et al.* [7] in the case of short infrared laser pulses ($\lambda = 2150$ nm and laser intensities of $I_0 = 1.3 \times 10^{11}$ and $6.5 \times 10^{11}$ W/cm$^2$) of 250 fs duration corresponding to 35 optical cycles. Similar bifurcation structures at above-threshold detachment have been noted by Krajewska *et al.* [27] in a nonperturbative Floquet study of H$^-$ negative ions in the vicinity of an eight-photon channel closure at an intensity of $1.76 \times 10^{10}$ W/cm$^2$ and a laser frequency of 0.0043 a.u. (i.e., $\lambda = 10.6$ $\mu$m).

#### *2. CEP sensitivity of PADs*

In Figs. 3(a)–3(g) we see that for each intensity and wavelength considered the PADs are symmetric about 90° for $\alpha = 0$ but for $\alpha = \pi/4$ the PADs are shifted to the left of 90° and for $\alpha = 3\pi/2$ the PADs are shifted to the right of 90°. Further calculations not shown here predict more generally that if $\alpha < \pi$ the PADs are shifted to the left and if $\alpha > \pi$ the PADs are shifted to the right. Figures 3(a)–3(i) demonstrate that the influence of the CEP becomes more significant with increasing wavelength and intensity. It is further noted that the PADs become increasingly asymmetric at the higher CEP values.

The positions of the maxima and minimum in the two-jetlike structures are observed to be highly dependent on the CEP. The degree of asymmetry of the two-jet structure is strongly correlated with the CEP. Our results show that structures in the PADs are extremely sensitive to variation in the CEP and thus measuring such distributions provides a robust tool for determining this phase.

### D. Photoelectron energy spectrum

Photoelectron energy spectra of negative H$^-$ ions near the two-photon detachment threshold are shown in Fig. 4. The main feature of the energy spectrum is the presence of peaks spaced by $\Delta\epsilon \approx \omega$. Since the photons in a short pulse are not monoenergetic the peaks are broader in comparison with the above-threshold peaks that one would observe in a long pulse. Figures 4(a)–4(c) show prominent two- and three-photon detachment channels. As the ponderomotive shift is increased with increasing intensity and wavelength the number of prominent excess photon detachment channels increases corresponding to the absorption of many more additional photons than necessary being absorbed at the onset of the continuum. In Figs. 4(g), 4(h), and 4(i) two, three, and four detachment channels, respectively, are clearly visible. Figures 4(f), 4(h), and 4(i) depict the onset of a fifth detachment channel. It is observed from Figs. 4(a)–4(i) that the increase in higher-order detachment channels is accompanied by increasing probability of closure of the two-photon channel. This happens because as the ponderomotive potential raises the continuum threshold, the minimum number of photons required to detach an electron from a negative ion increases when the laser intensity and/or wavelength is increased and this in turn leads to the closure of the lower photon detachment channels. This effect can be observed by noting that the peaks in Figs. 4(a)–4(i) tend to move to lower photoelectron energies as the intensity and/or wavelength increases. In particular at the highest wavelength of 2700 nm and laser intensity of $6.5 \times 10^{11}$ cm$^2$ [see 4(i)] the first peak disappears, as the ponderomotive shift makes detachment by two photons energetically impossible, although the absorption of excess photons is still allowed. Our results in Figs. 4(a)–4(i) show that the threshold for photodetachment increases as the ponderomotive shift increases. The minima observed in the nonmonotonic structures are caused by the adiabatic transition of the electrons to the final state in the laser field. This occurs at eight different instants of time over the duration of the three-cycle laser pulse and produces the quantum interference effects. The calculations here provide additional support for our findings in Secs. III B and III C of the present paper.

#### *1. Dependence of the energy spectrum on individual saddle points*

Also in Fig. 4 we analyze how the behavior of the energy spectrum is influenced by the number of saddle points included in the evaluation of the transition amplitude. It can be seen from Fig. 4 that at least roots 3–7 need to be included in

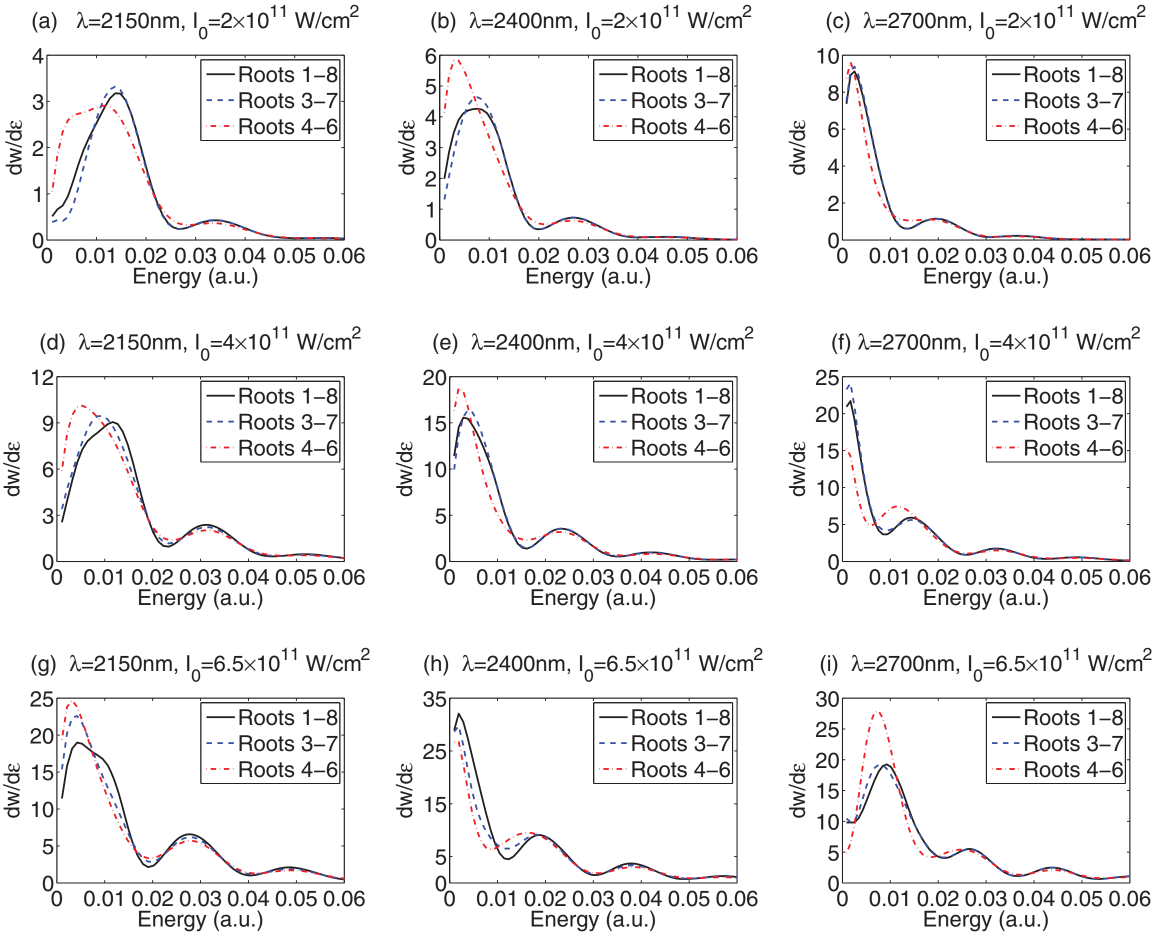

FIG. 4. (Color online) Photoelectron energy spectra calculated for a CEP of $\alpha = 0$ by including a different number of saddle points in the amplitude: three (4–6) shown by the red dash-dotted line, five (3–7) shown by the blue dashed line, and all eight (1–8) shown by the black line. The panels in each row represent wavelengths of 2150, 2400, and 2700 nm. The panels in each column correspond to laser intensities of $2 \times 10^{11}$, $4 \times 10^{11}$, and $6.5 \times 10^{11}$ W/cm$^2$.

the calculations to reproduce the full structure of the electron spectrum calculated at laser wavelengths of 2400 and 2700 nm. At $\lambda = 2150$ nm it is noted at lower electron energies, neglecting the first, second, and eighth saddle points leads to significant differences in the overall spectra compared to including all eight saddle points. This shows that saddle points 1, 2, and 8 play a stronger role in the photodetachment process at lower wavelengths and lower electron energies for each of the intensities considered. From Fig. 4 it is further noted that at the lower electron energies in each panel all roots need to be included to achieve 100% accuracy in the distributions. This is in contrast to recent results in Ref. [21] for photodetachment of $H^-$ negative ions in a laser pulse with five optical cycles and wavelength of 10.6 $\mu$m where one of the main results demonstrated that the pair of central saddle points 5 and 6, corresponding to the strongest part of the pulse, give over 90% contribution to the transition amplitude. In the present calculations, because the cycle is much shorter (i.e., $N = 3$) the contributions from each individual saddle point become more significant. This indicates that the side lobes of the electric field (which occur during ramp-on and ramp-off of the field) for $N = 3$ optical cycles make a dominant contribution to the transition amplitude in comparison to the longer pulse consisting of $N = 5$ where the side lobes contribute negligibly.

### 2. *Influence of the CEP on the energy spectrum*

Additional calculations presented in Ref. [26] show that as $\alpha$ is increased to $\pi/4$ (Fig. S5 in Ref. [26]) and $3\pi/2$ (Fig. S6 in Ref. [26]) the magnitude of the peaks in the spectrum varies but the position of the peaks and spacing of the peaks along the energy axis remain unaltered. Further calculations carried out (not shown) indicate that when the phase is 0, the middle roots 4,5 and 5,6 reproduce identical spectra. This result, however, is expected due to the symmetry around the fifth root at $\alpha = 0$ in Fig. 1. Similar simulations for $\alpha = \pi/4$ and $3\pi/2$ show that the pair of saddle points 4 and 5 gives a much larger contribution to transition amplitude for all wavelengths and intensities considered than the pair of saddle points 5 and 6. Again these findings are consistent with the symmetrical properties of the distributions in Fig. 1. Thus our results demonstrate that varying the CEP influences the impact that the contribution of individual saddle points make to the transition amplitude and thus controls the subsequent photodetachment dynamics of the energy spectra.

### E. Photoelectron momentum distributions

In Fig. 5 we present angle-resolved electron momentum distribution spectra of H$^-$ for laser wavelengths of 1800, 2150, 2400, and 2700 nm for the three peak laser intensities considered, $2 \times 10^{11}$, $4 \times 10^{11}$, and $6.5 \times 10^{11}$ W/cm$^2$, with a CEP of $\alpha = 0$. Additional results of the 2D photoelectron momentum distributions $(p_x, p_y)$ for CEP values of $\alpha = \pi/2$ and $3\pi/2$ are presented in Ref. [26] for the same set of laser wavelengths and intensities studied in Fig. 5. From Fig. 5 it is observed that for each of the four wavelengths considered at each intensity the momentum distributions are symmetric about both $p_x = 0$ and $p_z = 0$ for the CEP $\alpha = 0$. In Ref. [26] Figs. S7 and S8 show that for nonzero CEP values ($\alpha = \pi/2$ and $3\pi/2$) the momentum distributions become increasingly asymmetric about the $p_z$ axis for all intensities and wavelengths explored but retain their symmetry about the $p_x$ axis. These calculations further illustrate that the momentum distributions have perfect symmetry between the forward direction calculated at $\alpha = \pi/2$ and backward direction for $\alpha = 3\pi/2$ and that the symmetrical properties of the angularly resolved electron momentum distributions are highly correlated with the CEP. Our findings in Fig. 5 and in Figs. S7 and S8 of Ref. [26] are in excellent agreement with the analytical $S$-matrix calculations of Peng *et al.* [18] in the instances where our choices of parameters match.

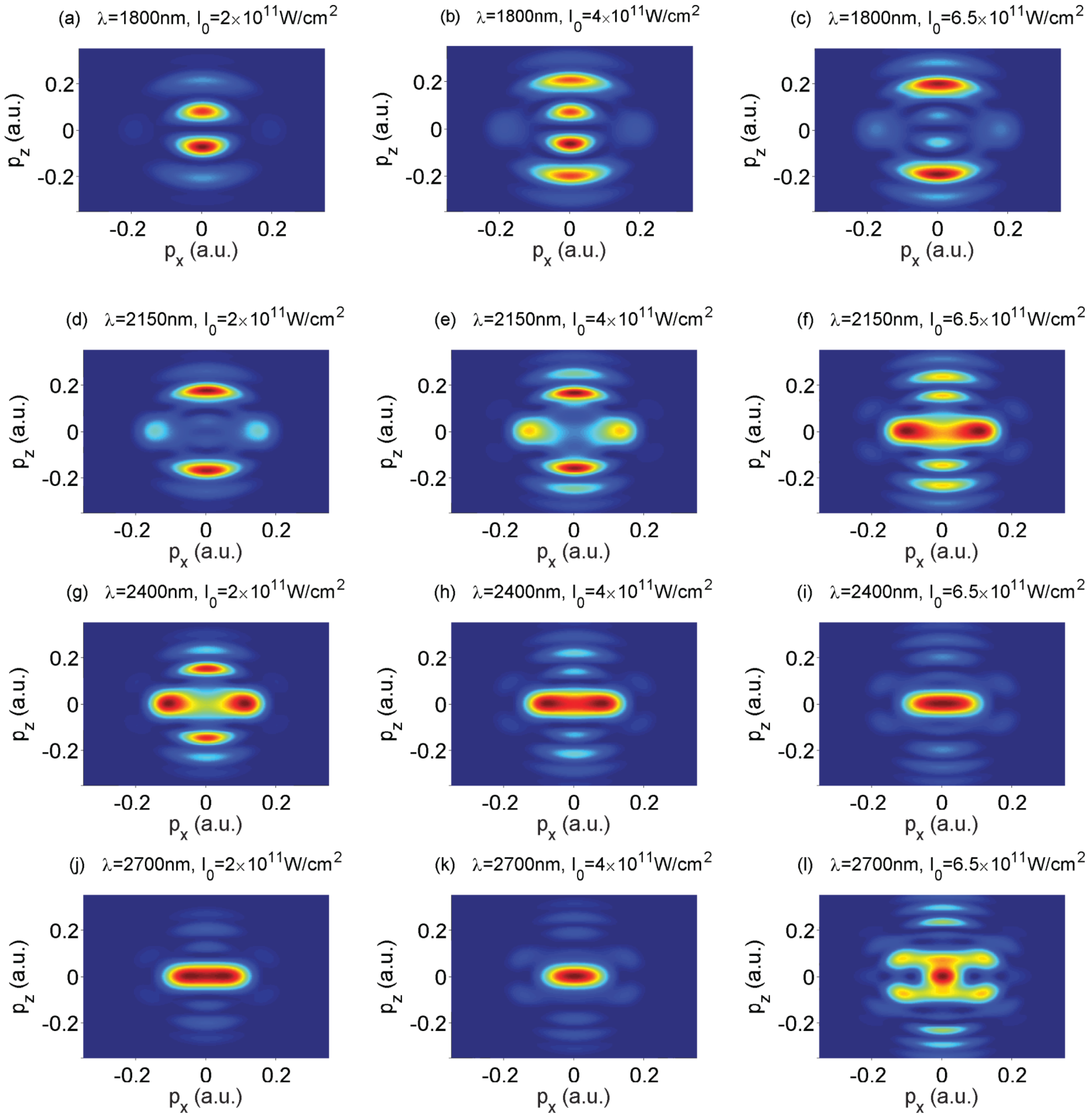

FIG. 5. (Color online) Two-dimensional momentum distributions of photoelectrons detached from H$^-$ corresponding to a CEP of $\alpha = 0$. The panels in each row correspond to peak laser intensities of $2 \times 10^{11}$, $4 \times 10^{11}$, and $6.5 \times 10^{11}$ W/cm$^2$. The panels in each column represent laser wavelengths of 1800, 2150, 2400, and 2700 nm, respectively. Momentum components perpendicular and parallel to the laser polarization axis are represented by $p_x$ and $p_z$, respectively.

### *1. Photon detachment probability peaks*

In Figs. 5(a), 5(d), 5(g), and 5(j) the momentum distributions are calculated at a laser intensity of $2 \times 10^{11}$ W/cm$^2$. It is observed that the detachment probability peaks for two- and three-photon detachment in Fig. 5(a) for $\lambda = 1800$ nm agree with the calculated values of 0.203 and 0.303 a.u. obtained using the formula $p_z = \sqrt{2(n\omega - U_p - E_b)}$, where $n$ is the number of photons absorbed and we have assumed $p_x = 0$. In Fig. 5(d) at $\lambda = 2150$ nm the observed peaks for two- and three-photon detachment occur at 0.151 and 0.256 a.u., respectively. At $\lambda = 2400$ nm in Fig. 5(g) the probability peaks for two-, three-, and four-photon detachment occur at 0.112, 0.225, and 0.298 a.u., respectively. For $\lambda = 2700$ nm the detachment probability peaks in Fig. 5(j) for two-, three-, and four-photon detachment occur at 0.045, 0.190, and 0.264 a.u., respectively.

Momentum distributions at a fixed laser intensity of $4 \times 10^{11}$ W/cm$^2$ are considered in Figs. 5(b), 5(e), 5(h) and 5(k). In Fig. 5(b) at $\lambda = 1800$ nm the observed probability peaks for two- and three-photon detachment occur at 0.192 and 0.296 a.u., respectively. With $\lambda = 2150$ in Fig. 5(e), the probability peaks for two- and three-photon detachment occur at 0.128 and 0.243 a.u., respectively. For a wavelength of $\lambda = 2400$ nm in Fig. 5(h) the detachment probability peaks for two-, three-, and four-photon detachment occur at 0.068, 0.206, and 0.284 a.u., respectively. At a higher wavelength of $\lambda = 2700$ nm two-photon detachment is not possible and in Fig. 5(k) the observed peaks for the three- and four-photon detachment occur at 0.161 and 0.244 a.u., respectively. The results for this set of laser parameters are also in good agreement with the theoretical calculations of Peng *et al.* [18].

Finally, the momentum distributions for electron spectra calculated at a laser field intensity of $6.5 \times 10^{11}$ W/cm$^2$ are examined in Figs. 5(c), 5(f), 5(i) and 5(l). Figure 5(c) shows that the observed probability peaks with $\lambda = 1800$ nm for two- and three-photon detachment occur at 0.177 and 0.286 a.u., respectively. In Fig. 5(f) at $\lambda = 2150$ the probability peaks for two-, three-, and four-photon detachment occur at 0.932, 0.226, and 0.305 a.u., respectively. For wavelengths of 2400 and 2700 nm two-photon detachment is not possible and in Fig. 5(i) the observed peaks for the three photon and four detachment occur at 0.181 a.u. and 0.266 a.u. and in Fig. 5(l) the observed peaks for the three-, four-, and five-photon detachment occur at 0.115, 0.217, and 0.285 a.u., respectively.

The observations noted above in Fig. 5 at the dominant frequency $\omega = \omega_1$ are consistent with our analysis and interpretation of the PADs in Sec. III C. However, as pointed out by Peng *et al.* [18], there are three different frequency components: $\omega_1 = \omega$, $\omega_2 = (1 + \frac{1}{N})\omega$, and $\omega_3 = (1 - \frac{1}{N})\omega$. This explains the origin of extra peaks that are observed in Fig. 5(a). Here single-photon detachment is possible at a laser intensity of $2 \times 10^{11}$ W/cm$^2$ with a wavelength of 1800 nm due to the frequency component $\omega_2 = 0.033\,76$ a.u., which yields an additional peak at $p_z = 0.087$ a.u. However, single-photon detachment at a laser intensity of $2 \times 10^{11}$ W/cm$^2$ at the higher wavelengths considered in Figs. 5(d), 5(g), and 5(j) is not possible with $\omega_2$. Note that in Fig. 5(d) single-photon detachment is possible with the frequency component $\omega_1 + \omega_3$ and yields a peak at $p_z = 0.094$ a.u. Similarly in Fig. 5(g), for $\lambda = 2400$ nm a single-photon detachment peak occurs at 0.088 a.u. with the frequency component $\omega_1 + \omega_3$ and in Fig. 5(j) this frequency component generates electrons with a momentum of 0.027 a.u. giving rise to a single-photon detachment peak.

Next we consider the frequency components at a laser intensity of $4 \times 10^{11}$ W/cm$^2$. In Fig. 5(b) at $\lambda = 1800$ nm, single-photon detachment becomes possible at a laser frequency of $\omega_2 = 0.033\,76$ a.u., which yields an extra peak at $p_z = 0.056$ a.u. Single-photon detachment beyond $\lambda = 1800$ nm with $\omega_2$ at this intensity is not possible. However, frequency combinations with $\omega_1 + \omega_2$ at $\lambda = 2150$ nm [Fig. 5(e)] makes two-photon detachment possible with a peak at $p_z = 0.175$ a.u. and one-photon detachment is possible at $\omega_1 + \omega_3$, which gives a peak at 0.049 a.u. Extra two-photon detachment peaks occur with $\omega_1 + \omega_2$ at $\lambda = 2400$ nm [Fig. 5(h)] and 2700 nm with $p_z = 0.131$ and 0.057 a.u., respectively [Fig. 5(k)]. Additionally, the combination of $\omega_1 + \omega_3$ gives two-photon detachment peaks at 0.088 a.u. for $\lambda = 2400$ nm and at 0.027 a.u. for $\lambda = 2700$ nm.

Finally we consider the frequency components at a laser intensity of $6.5 \times 10^{11}$ W/cm$^2$. In Fig. 5(c), with $\lambda = 1800$ nm, single-photon detachment is possible with the frequency combination $\omega_1 + \omega_3$ and produces electrons with a momentum of 0.12 a.u. In Fig. 5(f) at $\lambda = 2150$ nm the frequency component $\omega_1 + \omega_2$ produces another two-photon detachment peak at $p_z = 0.151$ a.u. and $\omega_1 + \omega_3$ produces another peak at $p_z = 0.123$ a.u. originating from two-photon detachment. In Fig. 5(i) electrons are generated with a momentum of 0.086 a.u. from the frequency mode $\omega_1 + \omega_2$ arising from the two-photon channel. In Fig. 5(l) the frequency combination of $\omega_1 + \omega_3$ leads to a two-photon peak at $p_z = 0.027$ a.u.

Most so-called single-wavelength lasers actually produce radiation in several modes having slightly different frequencies and this behavior is clearly revealed in these distributions. The results considered here also show that the combination of different frequency components can lower the threshold for photodetachment channels that are not admitted by the dominant frequency $\omega_1$.

## IV. CONCLUSION

We have applied the recent adiabatic saddle-point method of Shearer *et al.* [21] to study strong-field photodetachment of H$^-$ linearly polarized laser pulses with $N = 3$ optical cycles, of frequencies in the vicinity of the two-photon threshold where the ionization is tunnelinglike. Our work shows that application of the saddle-point method in the evaluation of the amplitude for a laser pulse with $N = 3$ optical cycles yields $2(N + 1)$ saddle points, all of which require inclusion in the transition amplitude to achieve a good degree of accuracy. This is in contrast to recent results [21] with $N = 5$, where it was only necessary to include the $N = 5$ inner saddle points to achieve the same level of accuracy. The present calculations and additional results in Ref. [26] therefore demonstrate that for very short pulses each individual saddle point makes an important contribution to the photodetachment amplitude. The distribution of the saddle points in the complex plane are also observed to be strongly dependent on (i) laser wavelength, (ii) laser intensity, and (iii) CEP.

The photoelectron differential detachment probabilities show detailed structures that signify photodetachment near the two-photon threshold. For instance, the distributions are characterized by a distinct central jet and two side lobes that are geometrically influenced by increasing wavelength and intensity. The geometric changes in the distribution are due to the bifurcation phenomenon that occurs in the vicinity of the two-photon channel closure. These distributions also display asymmetric behavior for nonzero CEP values, as shown in Ref. [26].

We have analyzed PADs for two- and three-photon absorption and shown that the PADs exhibit a show a high degree of dependence on the ponderomotive shift. This takes the role of the bifurcation parameter and determines the shape of the PADs. The PADs further demonstrate that the threshold for photodetachment increases with increasing laser intensity and increasing laser wavelength.

Our calculated electron energy spectra possess a well-pronounced nonmonotonic structure of peaks due to above-threshold ionization where each broad peak coincides with two-, three-, or four-photon absorption and is separated from its adjacent neighbor by the photon energy. The peaks are seen to occur as a manifestation of quantum interference effects. In addition we can identify the actual saddle points that lead to the quantum interference of electron paths in the final continuum state. The CEP has been shown to influence the contribution of individual saddle points to the final structure of the energy spectra, as illustrated in Ref. [26].

We have presented momentum distributions of photoelectron spectra for H$^-$ using our adiabatic saddle-point method. We have further demonstrated that the momentum distributions in the forward direction for a CEP $\alpha$ are the mirror image of those in the backward direction $2\pi - \alpha$ [26]. This asymmetrical behavior provides a reliable diagnostic tool for controlling the CEP of low-femtosecond laser pulses.

A key finding of this work shows that the momentum distributions contain signatures of the dominant frequency modes operating at our chosen range of laser parameters in the midinfrared region near the two-photon threshold. This study indicates that the 2D momentum distributions may serve as a useful probe in identifying all combinations of allowable frequency components that lead to photodetachment near the two-photon detachment threshold. Our findings confirm the $S$-matrix analysis of Ref. [18]. Finally, although our results are presented for H$^-$, they are also expected to be straightforwardly applicable to detachment by few-cycle lasers pulses of any negative ion having $s$-state valence electrons.

## ACKNOWLEDGMENTS

The authors gratefully acknowledge very useful and fruitful discussions with Dr. Gleb Gribakin. This work was supported in part by the Nuffield Foundation Undergraduate Research Bursary Scheme.

[1] T. Brabec and F. Krausz, Rev. Mod. Phys. **72**, 545 (2000).

[2] G. Sansone *et al.*, Science **314**, 443 (2006).

[3] D. B. Milošević, G. G. Paulus, D. Bauer, and W. Becker, J. Phys. B **39**, R203 (2006).

[4] F. Krausz and M. Ivanov, Rev. Mod. Phys. **81**, 163 (2009).

[5] P. B. Corkum and F. Krausz, Nature Phys. **3**, 381 (2007).

[6] G. F. Gribakin and M. Yu. Kuchiev, Phys. Rev. A **55**, 3760 (1997).

[7] R. Reichle, H. Helm, and I. Yu. Kiyan, Phys. Rev. Lett. **87**, 243001 (2001); Phys. Rev. A **68**, 063404 (2003).

[8] I. Yu. Kiyan and H. Helm, Phys. Rev. Lett. **90**, 183001 (2003).

[9] D. B. Milošević, A. Gazibegović-Busuladžić, and W. Becker, Phys. Rev. A **68**, 050702(R) (2003).

[10] M. V. Frolov, N. L. Manakov, E. A. Pronin, and A. F. Starace, J. Phys. B **36**, L419 (2003).

[11] B. Bergues and I. Yu. Kiyan, Phys. Rev. Lett. **100**, 143004 (2008).

[12] L. Bai, J. Zhang, X. Zhang, and Z. Xu, Phys. Rev. A **74**, 025402 (2006).

[13] L. V. Keldysh, Zh. Eksp. Teor. Fiz. **47**, 1945 (1964) [Sov. Phys. JETP **20**, 1307 (1965)].

[14] D. M. Volkov, Z. Phys. **94**, 250 (1935).

[15] S. X. Hu and A. F. Starace, Phys. Rev. A **68**, 043407 (2003).

[16] L.-Y. Peng, Q. Wang, and A. F. Starace, Phys. Rev. A **74**, 023402 (2006).

[17] S. Bivona, R. Burlon, and C. Leone, Opt. Express **14**, 12576 (2006).

[18] L.-Y. Peng, Q. Gong, and A. F. Starace, Phys. Rev. A **77**, 065403 (2008).

[19] T. P. Grozdanov and J. Jacimovic, Phys. Rev. A **79**, 013413 (2009).

[20] C. Arendt, D. Dimitrovski, and J. S. Briggs, Phys. Rev. A **76**, 023423 (2007).

[21] S. F. C. Shearer, M. C. Smyth, and G. F. Gribakin, Phys. Rev. A **84**, 033409 (2011).

[22] D. A. Telnov and Shih-I Chu, Phys. Rev. A **66**, 063409 (2002).

[23] A. Gazibegovic-Busuladzic, D. B. Milosevic, W. Becker, B. Bergues, H. Hultgren, and I. Y. Kiyan, Phys. Rev. Lett. **104**, 103004 (2010).

[24] E. E. Nikitin and B. M. Smirnov, *Atomic and Molecular Processes* (Nauka, Moscow, 1988).

[25] H. Hotop and W. C. Lineberger, J. Phys. Chem. Ref. Data **14**, 731 (1985).

[26] See Supplemental Material at http://link.aps.org/supplemental/10.1103/PhysRevA.85.063409 for additional calculations of the influence of laser intensities [$(2 \times 10^{11}) - (6.5 \times 10^{11})$ W/cm$^2$], midinfrared laser wavelengths (1800–2700 nm) and various values of CEP on (i) saddle point “smiles”, (ii) photoelectron differential detachment probabilities, (iii) photoelectron energy spectra, and (iv) photoelectron momentum distributions in strong-field photodetachment of H$^-$ by few cycle laser pulses.

[27] K. K. Krajewska, I. I. Frabrikant, and A. F. Starace, Laser Phys. **17**, 368 (2007).